

FURTHER DEVELOPMENT OF AN OPTIMAL DESIGN APPROACH APPLIED TO AXIAL MAGNETIC BEARINGS

V. Dale Bloodgood, Jr.

Old Dominion University, Norfolk, Virginia, US, dbloodgood@mindspring.com

Nelson J. Groom

NASA Langley Research Center, Hampton, Virginia, US, n.j.groom@larc.nasa.gov

Colin P. Britcher

Old Dominion University, Norfolk, Virginia, US, britcher@aero.odu.edu

ABSTRACT

Classical design methods involved in magnetic bearings and magnetic suspension systems have always had their limitations. Because of this, the overall effectiveness of a design has always relied heavily on the skill and experience of the individual designer. This paper combines two approaches that have been developed to aid the accuracy and efficiency of magnetostatic design. The first approach integrates classical magnetic circuit theory with modern optimization theory to increase design efficiency. The second approach uses loss factors to increase the accuracy of classical magnetic circuit theory. As an example, an axial magnetic thrust bearing is designed for minimum power.

NOMENCLATURE¹

A_g = Area of the pole pieces at the air gap

B = Flux density

B_r = Remanence flux of neodymium iron boron

F = Force

J = Current density

K_a = Actuator loss factor

K_f = Flux leakage factor

K_i = Coil mmf loss factor

L_g = Length of air gap

L_m = Permanent magnet thickness (on each pole piece)

V_c = Volume of the coil

η = Coil packing factor

μ_0 = Permeability of free space ($4\pi \times 10^{-7}$ H/m)

ρ = Resistivity of copper (2×10^{-5} $\Omega \cdot m$)

ω = Frequency of occurrence of disturbance force

INTRODUCTION

One of the most important factors to consider in the design of an active magnetic bearing is its power efficiency. Reducing the power consumption will reduce not only the operational costs, but also the acquisition costs. If the required power can be reduced, smaller, and therefore cheaper amplifiers and power supplies can be used. Reduction of power also lessens winding cooling requirements. While applications such as space based systems and small pumps for medical applications have the most to gain by reducing power requirements, more typical commercial systems can also be significantly improved.

Various approaches have been developed to aid the design of magnetic bearings. Parametric and systematic approaches have been developed to optimize the power to weight ratio of magnetic bearings [1] and to achieve minimum power [2]. These approaches are very useful in developing design strategies but do not typically yield specific solutions.

A direct minimum power optimization method was developed in 1998 [3]. However, it optimized an ideal model with no flux leakage or mmf losses considered. It yielded helpful design trends but did not give design-specific solutions. This approach has now been extended with the incorporation of finite element analysis.

Magnetic circuit theory is used to mathematically model the bearing. The weaknesses of classical circuit theory are overcome by including loss factors to account for flux leakage and magnetomotive force losses. The extended circuit theory is then incorporated into an optimization package.

¹. All equations are formulated in SI units

The bearing geometry that is being optimized is shown in Fig. 1. The system is being optimized for minimum power. The bearing is designed to support a load of 2025 N at an air gap of 4 mm. It is biased by a pair of neodymium iron boron permanent magnets placed on the poles of the stator. The remanent flux of the neodymium iron boron is 1.2 Tesla. The shaft clearance has a radius of 25 mm. The flux density in the iron is assumed to behave linearly up to a level of 1 Tesla. The maximum allowable current density of the windings is limited to 4 A/mm². The windings have a packing factor of 0.85. The overall volume of the coil is limited to 820 cm³.

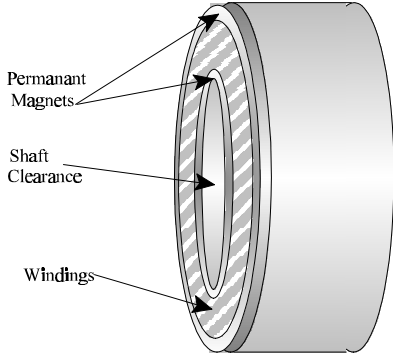


Figure 1: Axial Thrust Bearing Geometry

MODELING

Magnetic circuit theory was developed as an analogy to an electric circuit to model the behavior of a magnetic actuator. Several assumptions must be made for this analogy to hold: (1) there is no fringing or leakage flux, (2) there are no coil mmf losses, and (3) the permeability of the actuator core and return path is infinite. Applying magnetic circuit theory with these assumptions, the force applied to the rotating shaft by the magnetic actuator shown in Fig. 1 is [4],

$$F = \frac{\mu_0 A_g \left(NI + \frac{2B_r L_m}{\mu_0} \right)^2}{4(L_g + L_m)^2} \quad (1)$$

The accuracy of Eq. 1 depends on how well the assumptions are met. If the assumptions are reasonably well satisfied, the accuracy of the model can be within a few percent. However, in common practice the error can be much larger.

The accuracy can be greatly increased by relaxing these assumptions. This is done by introducing loss factors. Following the procedures outlined in [4], three factors can be introduced. The flux leakage around the magnetic circuit can be accounted for by the loss coefficient K_F .

The losses due to the finite permeability of the stator and armature can be combined to form the actuator loss coefficient K_a . The coil mmf loss can be accounted for by K_i . With the introduction of these terms into Eq. 1, the extended magnetic circuit model becomes,

$$F = \frac{\mu_0 A_g \left(K_i NI + \frac{2B_r L_m}{\mu_0} \right)^2}{4(K_a L_g + K_F L_m)^2} \quad (2)$$

The three coefficients are unknown at this point but can be determined from finite element analysis. If the actuator has already been built, the values can be determined from experimental data. The values of K_a and K_F are determined by rearranging Eq. 2 and setting $NI = 0$.

$$\begin{bmatrix} L_g & L_m \end{bmatrix} \begin{Bmatrix} K_a \\ K_F \end{Bmatrix} = \sqrt{\frac{A_g}{\mu_0 F_{FEA}}} B_r \ell_m \quad (3)$$

F_{FEA} is the force calculated by a finite element program. To accurately determine K_a and K_F , F_{FEA} must be determined at several different air gap distances. The more points that are used, the more accurate the solution. The validity of the solution is limited to the calculated range of air gap distances. The least squares solution for K_a and K_F can then be determined using the pseudo inverse.

$$\begin{Bmatrix} K_a \\ K_F \end{Bmatrix} = \begin{bmatrix} \begin{bmatrix} L_g & L_m \end{bmatrix}_1 \\ \vdots \\ \begin{bmatrix} L_g & L_m \end{bmatrix}_N \end{bmatrix}^{\#} \begin{Bmatrix} F_{FEA_1}^{-1/2} \\ \vdots \\ F_{FEA_N}^{-1/2} \end{Bmatrix} \sqrt{\frac{A_g}{\mu_0}} B_r L_m \quad (4)$$

Once K_a and K_F have been determined, K_i can be determined from Eq. 5.

$$K_i = 2 \sqrt{\frac{F_{FEA}}{\mu_0 A_g}} \left(\frac{K_a L_g + K_F L_m}{NI} \right) - \frac{2B_r L_m}{\mu_0 NI} \quad (5)$$

The appropriate choice of NI used to solve for K_i is important. If too small a value of NI is chosen, then the product $K_i NI \approx 0$, so the value of K_i becomes arbitrary. The most accurate method for determining K_i is to analyze several current levels near J_{max} and solve for the least squares solution. However, choosing a single value of NI near the upper limit of the operating range will provide a suitable value of K_i .

OPTIMIZATION

It is desired to optimize an axial magnetic thrust bearing for minimum power. The bearing will be designed to provide a specified force at a given gap distance. The bearing will be able to handle disturbance forces without exceeding the maximum allowable current density of the windings, and without saturating the magnetic flux within the circuit.

The power dissipated by a coil can be determined using the standard power equation,

$$P = \rho \eta J^2 V_c \quad (6)$$

At the operating point, the permanent magnets should provide a bias flux to carry the nominal load on the bearing. The power required by the coil will only be a factor when disturbance forces are present. For this particular case, it is assumed that the frequency of the disturbances follows a Gaussian distribution.

$$\omega(F) = \frac{1}{\sigma \sqrt{2\pi}} e^{-\frac{1}{2} \left(\frac{F - \bar{F}}{\sigma} \right)^2} \quad \sigma = \sqrt{\frac{\sum_{i=1}^n (F_i - \bar{F})^2}{n}} \quad (7)$$

The magnitude of the disturbance forces for this case have been set to $\pm 10\%$ of the operating force. Once the optimization code settles on an actuator configuration, the current density required to provide the designated loads can be written as a function of force. With this, the objective function can be written as,

$$f = \rho \eta V_c \int_{F_{min}}^{F_{max}} J^2(F) e^{-\frac{1}{2} \left(\frac{F - \bar{F}}{\sigma} \right)^2} dF \quad (8)$$

$$\approx \rho \eta V_c \frac{0.2 \bar{F}}{n-1} \sum_{i=1}^n J^2(F_i) e^{-\frac{1}{2} \left(\frac{F_i - \bar{F}}{\sigma} \right)^2}$$

The performance characteristics of the actuator are controlled through the constraint equations. The bearing is being designed to support a specified load at a specified air gap. This introduces the equality constraint.

$$F = \frac{\mu_0 A_g \left(K_i NI + \frac{2B_r L_m}{\mu_0} \right)^2}{4(K_a L_g + K_F L_m)^2} \quad (9)$$

There are three additional inequality constraints that must be added to the system. The first requires that the current density required to support the load at the high and low end of the design range remain below J_{max} . The equation

can be developed by substituting $NI = \eta A_c J$ into Eq. 9 and solving for J .

$$J_{max} \geq \left| \sqrt{\frac{4F_{Max,Min}}{\mu_0 A_g} \left(\frac{K_a L_g + K_F L_m}{\eta A_c} \right) - \frac{2B_r L_m}{\mu_0 \eta A_c}} \right| \quad (10)$$

The second inequality constraint requires that the flux density within the iron remains below the saturation level, 1 Tesla, at every point within the circuit. To avoid contractions where the flux may saturate, the minimum cross sectional area of the iron was specified to equal the pole area at all points.

$$B_{sat} \geq \frac{\mu_0 \left(K_i NI_{max} + \frac{2B_r L_m}{\mu_0} \right)}{2(K_a L_g + K_F L_m)} \quad (11)$$

The final constraint requires the volume of the actuator to remain finite. For this case the maximum volume was limited to 820 cm³.

$$V_{MAX} \geq V \quad (12)$$

The coil geometry has been divided as shown in Fig. 2. Because the cross sectional area of the circuit was specified to equal the pole area, the outer wall thickness t , and the back wall thickness b , can be written in terms of the other variables. The design vector can therefore be reduced to 5 variables,

$$\bar{x} = [r \quad w \quad h \quad L_m \quad J] \quad (13)$$

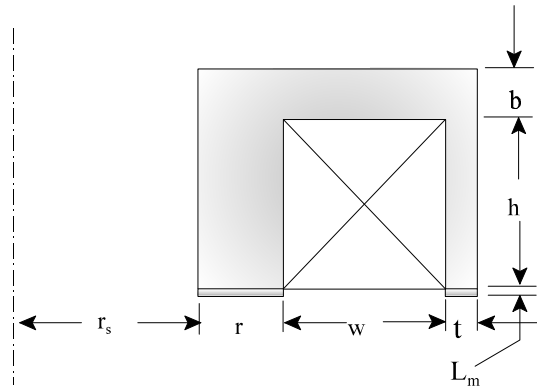


Figure 2: Description of Actuator Geometry

The geometry of the actuator is not known at the start of the optimization process, so no loss factors can be calculated. An estimation of the final optimization space can be determined by setting all the loss coefficients to 1. Thus, the assumptions associated with classical circuit theory are active and it is found that the actual force

produced by the coil will typically be less than that predicted by the optimized solution.

The ideal model is optimized and a solution is obtained. The actuator is then analyzed using finite element analysis and the loss factors are obtained. These loss factors are then introduced into the optimization code and the extended circuit theory model is optimized. Assuming that the addition of the loss factors does not significantly change the coil geometry, the optimum actuator configuration is then determined. If the geometry does change significantly, additional steps will be needed to determine precise values of K_a , K_F , and K_i for the optimizer.

IMPLEMENTATION OF EQUATIONS

MATLAB's optimization toolbox version 5.3. was chosen to optimize the axial thrust bearing. The package uses the Sequential Quadratic Programming Method (SQP), which is ideally suited for nonlinear problems with nonlinear constraints. SQP uses the BFGS quasi-Newton method to approximate the Hessian of the Lagrangian function. The new Hessian is used to solve a Quadratic Programming subproblem in order to determine the best search direction and step length [5]. MATLAB also offers the advantage that the optimization toolbox is commercially available.

The finite element modeling was performed using Vector Fields PC-OPERA 2D. Axial symmetry was used with the modified $r \times a$ potential [6]. The calculations were performed using quadratic elements with non-linear material properties. The iron was modeled using the standard material BH curve supplied by Vector Fields, and the Neodymium Iron Boron had a remanent flux of 1.2 Tesla and a coercivity of 9.7×10^5 A/m.

There was some dependence upon the initial conditions to whether or not the optimizer would converge. When it did converge it was always to the same solution. When it did not converge, the initial conditions were randomly perturbed by $\pm 10\%$ until the solution converged. To keep the units consistent, all lengths were implemented in the optimization code as meters. Accordingly, the current density was scaled to vary between 0 and 1 since the order of magnitude of r , w , h , and L_m was 0.1 while the order of J_{max} was $1e6$.

Once the optimizer settled on a configuration six finite element runs were used to determine the loss factors. K_a and K_F were determined using five air gap lengths about the operating point, $L_g = 3.0, 3.5, 4.0, 4.5,$ and 5.0 mm. K_i was determined by setting $NI = \eta A_c J_{max}$.

DISCUSSION OF RESULTS

The ideal model was optimized with the loss factors set to 1 and a minimum power configuration was found. The resulting configuration and actual loss factors are given as Design-A in Table 1. The configuration delivered a zero power force of 1778 N, 12% below the desired value. The loss factors were then used in the optimization loop to develop the extended optimized model, Design-B. The addition of the constant loss factors only increased the zero power force to 1800 N, an improvement of less than 2%. The ideal and extended models of Design-A, along with the extended model of Design-B, and the finite element results are shown in Fig. 3.

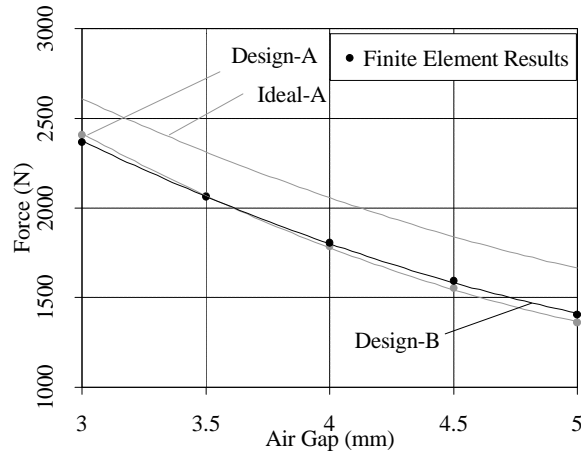


Figure 3: Actuator Performance for Designs A and B

The addition of the loss factors in the extended model of Design-A increased the accuracy of the formulation from 15% to 0.3% when compared to the finite element results.

Including the constant loss factors in the optimization loop had a negligible effect on the desired performance level. This is because the extended optimized design varied significantly from the ideal. The loss factors K_a , K_F , and K_i for Design-B had an error of 10%, 2%, and 1%, respectively, when compared to the actual values. This is due to the optimizer not being aware of the additional losses, due to the changes in the actuator geometry, during the optimization process.

Design-B had a narrower pole face which increased flux leakage. It also had a thicker permanent magnet which increased the affective air gap reluctance. The increase in the conductor height, h , additionally increased the reluctance of the iron path. The full effect of these changes were not accounted for in the optimization process and resulted in a poor configuration. Thus, the addition of constant loss factors in the optimization loop does not provide a global minimum power configuration.

To dynamically include the loss factors in the optimization loop the loss factors must change with the geometry of the actuator and accurately represent the loss characteristics. Currently, a method is under development that will provide an estimation of the loss factors over a range of possible actuator geometries. This technique is still being developed and is the subject of future work. Using a preliminary approach to including estimated loss factors into the optimization loop resulted in Design-C, listed in Table 1.

TABLE 1: Optimization Results and Loss Factors

Design	r (mm)	w (mm)	h (mm)	L_m (mm)	t (mm)	b (mm)	K_a	K_F	K_i
A	25.1	17.4	19.8	4.9	12.8	18.8	1.363	0.841	1.072
B	22.2	19.5	23.4	6.5	11.1	17.0	1.508	0.862	1.082
C	26.6	17.4	15.9	5.00	13.5	19.7	1.319	0.840	1.071

The performance results are shown in Figs. 4 and 5. The actuator geometry for Design-C is illustrated in Fig. 6.

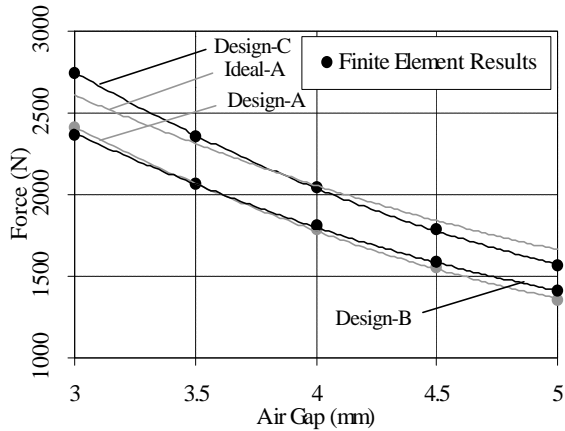


Figure 4: Actuator Performance for Designs A, B, and C at $NI = 0$

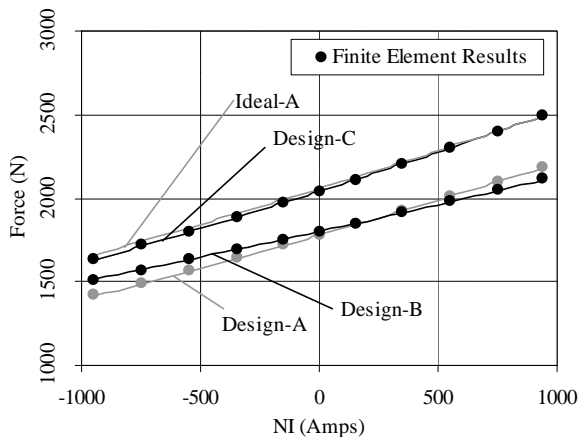


Figure 5: Actuator Performance for Designs A, B, and C at $L_g = 4mm$.

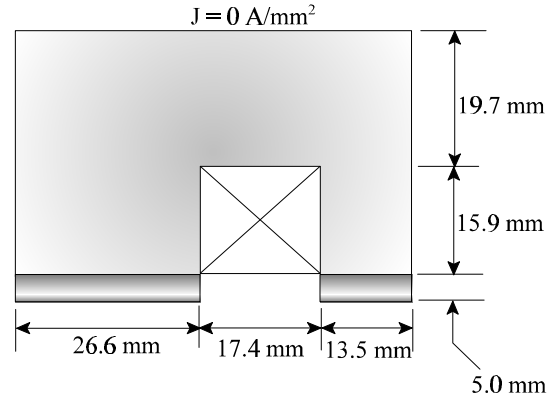


Figure 6: Optimized Actuator Configuration

Comparing designs A and C reveals several trends. The pole area of Design-C increased which reduced the flux leakage. It also increased the volume of the permanent magnet which was necessary to compensate for the losses between the ideal model and the extended model. The permanent magnet volume increased while keeping the magnet thickness essentially the same, reducing the apparent gap reluctance. Also, the height of the conductor was reduced. This lessened the volume of the copper windings and reduced the reluctance of the iron path.

Inclusion of the varying loss factors in the optimization loop resulted in a zero current force of 2046 N, 1% from desired. With the varying loss factors in the optimization loom, the actuator performance improved by 268 N at the zero current condition for the same size actuator. The accuracy of this model is evident by how well the Design-C model predicts the finite element results in Figs. 4 & 5.

The optimization routine converged to a minimum power configuration. The solution can be checked by perturbing the design variables and analyzing the objective function. The solution is presumed to be the global minima within the accuracy of the estimated loss factors. For Design-C, the estimated loss factors K_a , K_F , and K_i varied from the exact values by 1.4%, 1.4%, and 3% respectively. Improvements to these values would slightly modify the optimum results but should not produce any significant changes.

By reducing the reluctance losses and flux leakage at the gap, the actuator loss factor decreased by 3%. The flux leakage factor and coil mmf loss factor did not vary much between the two designs. This was because the slight variations between the two configurations did not dramatically change the overall actuator characteristics.

Efficiency trends evident to the optimizer for the ideal case and the extended case are different. In the ideal model, the winding volume is minimized by increasing the height of the conductor and reducing the mean radius. This leads to a tall-narrow design that reduces power by reducing winding volume. In the extended model with the varying loss factors, the optimizer is aware that this design increases the flux loss and converges to a short-wide design. The same opposing efficiency trends are evident in the permanent magnet results. The tall-narrow design increased the permanent magnet volume by making the magnet thicker. In Design-C, the permanent magnet volume was increased by making the magnet wider.

CONCLUSIONS

This design method provides a unique approach for the design of magnetic bearings. Not only is the final design optimally suited to the specifications of the designer, but it also results in an accurate model if the finite element results are accurate. In the axial thrust bearing example covered in this paper, the extended circuit model had an accuracy of 99%.

The method allows design constraints to be easily incorporated. Examples include constraints on flux density, current density, stiffness, volume, and geometric constraints. While in this case the bearing was optimized for minimum power, the objective statement could be easily modified to maximize or minimize force, stiffness, weight, volume, as well as many other possibilities.

The use of constant loss factors to estimate losses in the optimization loop did not prove successful. The minimum power trends within the ideal and the extended models oppose each other. In order to optimize the realistic model, the variation of the loss factors with geometry must be accounted for.

In the example, the combined use of the optimization code and variable loss factors increased the zero power force by 268 N. The performance was improved with no increase in actuator volume and only a slight increase in permanent magnet volume.

ACKNOWLEDGMENTS

This work was supported by the NASA Graduate Student Researchers Program and the Virginia Space Grant Consortium.

REFERENCES

1. Malone, C. L., "Power to Weight Optimization for Magnetic Bearings," Mag '93: Magnetic Bearings, Magnetic Drives and Dry Gas Seals Conference & Exhibition, Alexandria, Virginia, July 1993.
2. Klesen, C., Nordmann, R., Schönhoff, U., "Design of a Minimum Current Magnetic Bearing," 5th International Symposium On Magnetic Suspension Technology, Santa Barbara, CA, December 1999.
3. Bloodgood, V. D., "Design Optimization of Magnetic Bearings and Magnetic Suspension Systems." Masters Thesis, Old Dominion University, December 1998.
4. Groom, N. J., Bloodgood, Jr., V. D., "A Comparison of Analytical and Experimental Data for A Magnetic Actuator", NASA TM.
5. Coleman, T. F., Branch, M. A., Grace, A., "Optimization Toolbox for use with MATLAB," Users guide, Version-2, January 1999.
6. "PC-OPERA, Software for Electromagnetic Design," Vector Fields Reference manual, Version 01-97-F4, 1997.